Analyst

PAPER

A comparative study of carbon–platinum hybrid nanostructure architecture for amperometric biosensing†

Cite this: *Analyst*, 2014, **139**, 660

Diana C. Vanegas,[ab] Masashige Taguchi,[a] Prachee Chaturvedi,[a] Stephanie Burrs,[a] Michael Tan,[c] Hitomi Yamaguchi[c] and Eric S. McLamore*[a]

Carbon and noble metal nanomaterials exhibit unique properties that have been explored over the last few decades for developing electrochemical sensors and biosensors. Hybridization of nanometals to carbon nanomaterials such as graphene or carbon nanotubes produces a synergistic effect on the electrocatalytic activity when compared to either material alone. However, to date there are no comparative studies that directly investigate the effects of nanocarbon concentration and nanocomposite arrangement on electron transport. This comparative study investigated the efficacy of various platinum–carbon hybrid nanostructures for amperometric biosensing. Electroactive surface area, sensitivity towards hydrogen peroxide, response time, limit of detection, and surface roughness were measured for various hybrid nanomaterial arrangements. Both design factors (nanocarbon concentration and network arrangement) influenced the performance of the reduced graphene oxide-based platforms; whereas only nanomaterial arrangement affected the performance of the carbon nanotube-composites. The highest sensitivity towards hydrogen peroxide for reduced graphene oxide nanocomposites (45 ± 3.2 μA mM^{-1}) was measured for a graphene concentration of 2 mg mL^{-1} in a "sandwich" structure; nanoplatinum layers enveloping the reduced graphene oxide. Likewise, the best carbon nanotube performance toward H_2O_2 (49 ± 1.4 μA mM^{-1}) was measured for a sandwich-type structure with nanoplatinum. The enhanced electrocatalytic activity of this "sandwich" structure was due to a combined effect of electrical junctions formed amongst nanocarbon, and nanocomposite soldering to the electrode surface. The top-down carbon–platinum hybrid nanocomposites in this paper represent a simple, low-cost, approach for formation of high fidelity amperometric sensors with remarkable performance characteristics that are similar to bottom-up fabrication approaches.

Received 9th September 2013
Accepted 4th December 2013

DOI: 10.1039/c3an01718d

www.rsc.org/analyst

Introduction

Carbon and metal nanomaterials have been widely used in the last decade for electroanalytical applications due to their unique electrocatalytic properties, vast surface area-to-volume ratio, robust mechanical strength, and excellent biochemical stability.[1–4] Nanomaterials such as reduced graphene oxide, carbon nanotubes, and metal nanoparticles have been extensively used as electrocatalytic platforms in electrochemical biosensors (*e.g.*, amperometric, potentiometric, and impedimetric) to improve sensitivity, response time, and limit of detection. There have been a wide array of graph-from (*i.e.*, bottom-up) and graph-onto (*i.e.*, top-down) synthesis approaches for preparation of carbon–metal hybrid nanocomposites.[5,6] In general, graph-from approaches are preferred by most labs, although these techniques can be cumbersome and require specialty equipment. Some graph-onto approaches for sensors have demonstrated electron transport rates that are similar to graph-from synthesized sensors.[7,8]

Several studies suggest a synergistic electrocatalytic effect resulting from the conjugation of carbon nanomaterials with metal nanoclusters[9–13]. Functionalization of reduced graphene oxide or carbon nanotubes with nanometals helps maintain interplanar spacing and can also act as an electrical junction between nanoparticles and/or the electrode surface.[14] For instance, Shi *et al.*[15] reported a microbiosensor platform composed of graphene oxide and amorphous nanoplatinum (*i.e.*, Pt-black). The composite yielded a sensitivity towards hydrogen peroxide of 4.8 μA mM^{-1}. The combination of graphene oxide and platinum black was more efficient than either nanomaterial alone in enhancing electron transport. McLamore *et al.*[11] demonstrated the use of platinum black decorated

[a]*Department of Agricultural & Biological Engineering, University of Florida, 1741 Museum Road, Gainesville, FL, USA; Web: emclamor@ufl.edu; Tel: +1 352 392 1864*
[b]*Department of Food Engineering, Universidad del Valle, Ciudad Universitaria Meléndez, Edif. 338, Cali, Colombia, USA*
[c]*Department of Mechanical and Aerospace Engineering, University of Florida, 226 MAE-B Building, Gainesville, FL, USA*

† Electronic supplementary information (ESI) available. See DOI: 10.1039/c3an01718d

multiwalled carbon nanotubes (MWCNT) as a nanomaterial platform for glucose biosensing. The nanomaterial-mediated micro-biosensor showed sensitivity towards glucose of 531 pA mM^{-1}, which was significantly larger than most previously reported glucose micro-biosensors. Tsai & Hong[13] fabricated a Pt–MWCNT–Nafion nanocomposite onto a glassy carbon (GC) electrode for electrochemical oxidation of methanol. The Pt–MWCNT–Nafion platform had higher oxidation of methanol than the Pt-coated GC electrode and the Pt–Nafion-modified electrode. Claussen *et al.*[16] described two hybrid nanomaterial biosensor platforms, based on networks of single-walled carbon nanotubes conjugated with either palladium nanocubes (Pd nanocube–SWCNT) or platinum nanospheres (Pt nanosphere–SWCNT). These platforms were functionalized with the enzyme glutamate oxidase to create glutamate biosensors. The Pt nanosphere–SWCNT biosensor exhibited significantly enhanced performance compared to previously reported glutamate biosensors, low detection limit (4.6 nM), and a wide linear sensing range (50 nM to 1.6 mM). Claussen *et al.*[16] suggested that the unique nanoscale-environment of the Pt nanosphere–SWCNT hybrid biosensor could act synergistically to accurately monitor neurotransmitter release/uptake by neurons.

Even though enhanced electrocatalysis of metal–nanocarbon composites has been well established, no research efforts have clearly assessed the effect of nanoparticle density and arrangement on electrochemical performance in a detailed comparative study. This study presents common methodologies for developing rapid/low-cost platinum–nanocarbon hybrid nanocomposites for amperometric sensing. The assembly of hybrid nanomaterial platforms based on graphene oxide, multiwalled carbon nanotubes, and nanoplatinum was investigated. The effect of nanocarbon concentration and nanomaterial network arrangement on amperometric performance was studied in detail.

Experimental

Materials and reagents

Single-layered graphene oxide powder (GO) (height: 0.7–1.2 nm; purity: >99 wt%; manufacturing method: modified Hummers, with no metal catalyst) and multiwall carbon nanotubes powder (MWCNT) (outside diameter: 8–15 nm; purity: 95 wt%; length: 10–50 mm; manufacturing method: catalyzed chemical vapor deposition) were purchased from Cheap Tubes Inc. (Brattleboro, USA) and used as received. Dimethylformamide (DMF), and lead acetate 30% w/v were obtained from Fisher Scientific (Pittsburgh, USA). Chloroplatinic acid 8 wt% was procured from Sigma-Aldrich (St. Louis, USA). Hydrogen peroxide 35 wt%, and potassium nitrate (KNO_3) were acquired from Acros organics (New Jersey, USA). Potassium ferrocyanide trihydrate ($K_3Fe(CN)_6$) was purchased from EMD chemicals (Billerica, USA). Phosphate buffer saline (PBS) was procured from Mediatech, Inc. (Manassas, USA).

Hybrid nanomaterial fabrication

Pt/Ir working electrodes (BASI MF-2013, 1.6 mm diameter, 7.5 cm length, 6 mm shaft diameter, CTFE plastic body) were used to test all nanomaterial platforms based on the methods in Shi *et al.*[17] and McLamore *et al.*[11] Prior to modification, the Pt electrodes were polished with 3, and 1 μm polycrystalline diamond suspensions (Buehler®, USA), rinsed with methanol, and then polished with 0.05 alumina slurry (Buehler®, USA). Finally, electrodes were ultrasonicated in deionized water for 15 min. Amorphous nanoplatinum clusters (nPt) were deposited *via* electrodeposition in a solution of 0.728% chloroplatinic acid and 0.002% lead acetate. The Pt/Ir electrode was connected to the cathode on a DC power supply (Electro Industries, USA), and a bare platinum wire (0.3 mm diameter; Alfa Aesar, Ward Hill, USA) was connected to the anode. A 10 V constant voltage was applied for 90 seconds based on previously reported methods.[12,15,16] GO and MWCNT solutions were prepared in DMF to concentrations of 1, 2, and 3 mg mL^{-1}. All solutions were ultrasonicated for 15 minutes. 1 μL of the resulting solution was drop-casted on the tip of the Pt/Ir electrodes and dried overnight. GO was reduced during the ultimate electrodeposition of nPt in chloroplatinic acid, which is consistent with Shi *et al.*[15]

Eight nanomaterial platform configurations were assembled on the electrode surfaces: Pt/Ir–MWCNT, Pt/Ir–nPt–MWCNT, Pt/Ir–MWCNT–nPt, Pt/Ir–nPt–MWCNT–nPt, and analogously Pt/Ir–GO, Pt/Ir–nPt–GO, Pt/Ir–RGO–nPt, Pt/Ir–nPt–RGO–nPt. Fig. 1 shows a schematic of the hybrid nanomaterial configurations. The resulting experimental designs are 3 × 4 factorials (3 carbon concentrations by 4 nanomaterial configurations) with three observations per cell.

Electrochemical analysis

Electrochemical characterization was performed using a 3 electrode cell stand (C-3,BASi, West Lafayette, IN). Cyclic voltammetry was carried out in 4 mM $Fe(CN)_6$/1 M KNO_3 solutions at initial potential of 0 mV and switching potential of 800 mV, *versus* a Ag/AgCl reference electrode (RE-5B with flexible connector, BASi, West Lafayette, IN) with 10 seconds quiet time, and scan rates of 20, 50, 100, 125, 150, and 200 mV s^{-1}. The electroactive surface area of each nanomaterial mediated electrode was determined using the Randles–Sevcik equation:[18]

$$i_p = (2.69 \times 10^5) n^{3/2} D^{1/2} C A v^{1/2} \quad (1)$$

where i_p is the oxidation peak obtained from the cyclic voltammogram, n is the number of transferred electrons in the redox reaction, D is the diffusion coefficient, C is the molar concentration of the working solution, A is the electroactive surface area of the electrode and v is the potential scan rate. Since n, D, and C are known properties of the working solution, A was calculated from the slope of the Cottrell plot (i_p *versus* $v^{1/2}$).

DC potential amperometry (DCPA) was conducted in PBS (pH 7.4) at a working potential of +500 mV *versus* Ag/AgCl reference electrode with a sampling rate of 1 kHz. After 5 minutes of polarization, the current output was measured at constant potential while successively injecting hydrogen peroxide (H_2O_2) in the stirred working solution (450 rpm) at 60 seconds intervals to allow the electrical signal to reach steady state. The dynamic DCPA curves were used to evaluate the

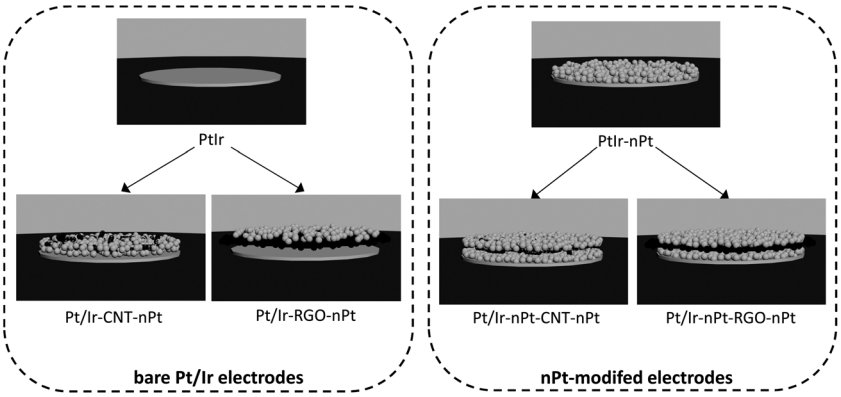

Fig. 1 Schematic representation of nanomaterial platforms assembled on platinum/iridium (Pt/Ir) electrodes: (left) carbon nanotubes (CNT) or reduced graphene oxide sheets (RGO) were first deposited at concentrations of 1,2, and 3 mg mL^{-1}, followed by electrodeposition of nano-platinum clusters (nPt). (right) A nPt–nanocarbon–nPt "sandwich" was formed at nanocarbon concentrations of 1,2, and 3 mg mL^{-1}.

performance of the nanomaterial mediated electrodes in terms of sensitivity, response time, and lower limit of detection.

Sensitivity was calculated from the slope of the linear portion of the calibration curves. Response time (t_{95}) was obtained by averaging the 95% steady state response time of three successive step changes over the linear range tested (approximately 0–300 μM H_2O_2). The steady state response was determined by performing non-linear regression over single step changes in concentration (exponential rise to maximum/single, 3 parameter/SigmaPlot 12.0).

The lower limit of detection (LOD) was calculated using the 3σ method.[19,20]

Statistical analysis

All electrochemical measurements were performed in triplicate. Analysis of variance (ANOVA model I) was performed in order to judge whether or not any effects in electrochemical performance are statistically significant.[21]

Imaging and elemental characterization

Morphological characterization of the nanomaterials was conducted *via* scanning electron microscopy (SEM) and scanning white light interferometry (SWLI). SEM images were taken on a JEOL 5600 LV, with accelerating voltage of 12–15 kV. SWLI profiles (707 μm × 530 μm area) were obtained with a Zygo Newview 7200 with a 20× by 2× objective. A Gauss Spline filter (band-pass mode) with cut-off wavelength of 20 μm (low pass) and 0.83 μm (high pass) was applied. Elemental analysis of the nanomaterial platforms were conducted by electron dispersive X-ray spectroscopy (EDS) using an OXFORD INCA 250 operating at 75 kV.

Results & discussion

Fig. 2A shows a representative cyclic voltammogram of a Pt/Ir–nPt–RGO–nPt modified electrode. Each CV in this study exhibited a response characteristic of a reversible couple with well-defined redox peaks, indicating a diffusion controlled reaction at the electrode-solution interface in which the diffusion layer was smaller than the surface area of the electrode. Based on eqn (1), Cottrell plots were prepared to calculate the electroactive surface area of each nanomaterial-modified electrode (a representative plot of a Pt/Ir–nPt–RGO–nPt modified electrode is shown in Fig. 2B).

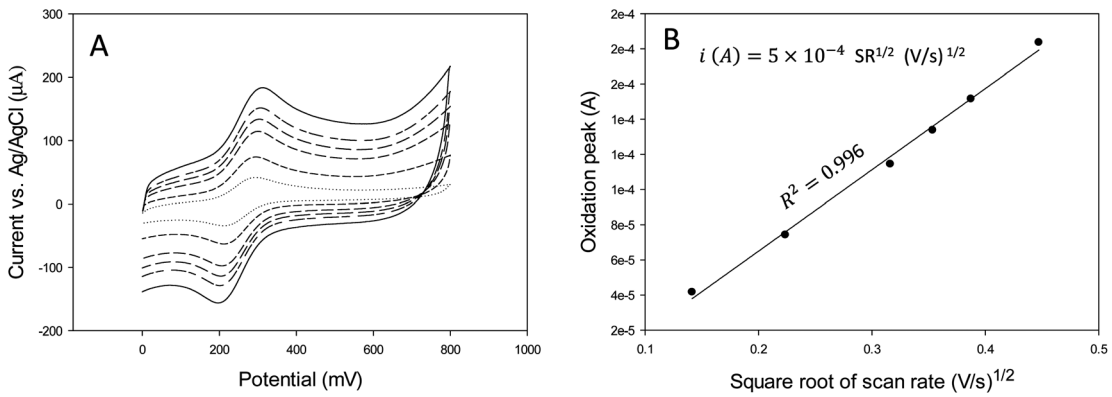

Fig. 2 (A) Representative cyclic voltammograms of a Pt/Ir–nPt–RGO–nPt modified electrode in 4 mM $Fe(CN)_6$/1 M KNO_3 solution at different voltage scan rates. The magnitude of the electrical signal increases as the scan-rate increases. (B) Characteristic Cotterell plot of a Pt/Ir–nPt–RGO–nPt modified electrode. The calculated electroactive surface area was 0.18 cm^2.

A typical dynamic DCPA curve of a Pt/Ir–nPt–RGO–nPt electrode is displayed in Fig. 3A. Each injection of H_2O_2 produced a current signal which was proportional to the bulk concentration of H_2O_2 in the working solution. Fig. 3B shows a characteristic steady state calibration curve within the linear range of the Pt/Ir–nPt–RGO–nPt electrode. A correlation coefficient (R^2) higher than 0.99 was obtained in each linear regression for the calibration curves of all nanomaterial mediated electrodes. Hydrogen peroxide is the product of several enzyme-catalyzed reactions; oxidative amperometry is the most common type of enzymatic biosensor. Thus, sensor platforms which demonstrate detection of H_2O_2 with high sensitivity and low detection limit are desirable. These nanomaterial composites could serve as platforms for enzymatic biosensors when combined with oxidative enzymes.

MWCNT–nPt hybrid nanomaterials

Fig. 4A shows the electroactive surface area of all MWCNT–nPt hybrid electrodes in this study. There were no significant differences in electroactive surface area between the hybrid nanomaterials tested. Both design factors (nanomaterial configuration and MWCNT concentration) had the same effect on the response variable (electroactive surface area) ($p > 0.05$). The highest electroactive surface area was 0.07 ± 0.015 cm^2, which was about 3.5 times higher than a bare Pt/Ir electrode.

The mean sensitivity towards H_2O_2 for all MWCNT modified electrodes is shown in Fig. 4B. Analysis of variance indicated that only the nanomaterial configuration had a significant effect ($p < 0.05$) on the amperometric sensitivity (see ESI, Table 1† for details). Regardless of MWCNT concentration, the highest sensitivity was measured for the Pt/Ir–MWCNT–nPt (49 ± 1.4 μA mM^{-1}) and the Pt/Ir–nPt–MWCNT–nPt (51 ± 15.4 μA mM^{-1}) platforms. These sensitivity values were approximately 10 times more sensitive than a bare Pt/Ir electrode (see ESI, Fig. 1† for representative calibration curves of the MWCNT-based nanomaterial platforms).

Hybrid nanocomposites based on carbon nanotubes and metal nanoparticles such as cobalt, gold, palladium, and platinum have been widely used for development of electrochemical devices.[10,13,16,22,23] These nanocomposites have demonstrated enhanced electrocatalytic properties than either carbon nanotubes, or nanometals alone. Several research groups have suggested that the edge-plane defect sites on the surface of the nanotubes can serve as nucleation sites for the formation of metal nanoclusters. These nanoclusters are thought to establish Ohmic contacts along the nanomaterial network, facilitating formation of high on-state currents.[23–26]

RGO–nPt hybrid nanomaterials

Fig. 5A shows the average electroactive surface area of the graphene–Pt hybrid nanomaterials. The bare Pt/Ir electrode with GO drop cast on the surface (Pt/Ir–GO) had the lowest electroactive surface area (0.007 ± 0.002 cm^2) of all the nanomaterial configurations tested. The Pt/Ir–nPrt–GO hybrid had a slightly improved electroactive surface area (0.033 ± 0.015 cm^2), although this architecture was not a significant improvement over GO-modified electrodes. The highest electroactive surface area was exhibited by the 2 mg mL^{-1} Pt/Ir–nPt–RGO–nPt modified electrode (0.148 ± 0.064 cm^2) being at least 7.5 times larger than a bare Pt/Ir electrode (0.019 ± 0.003 cm^2).

There were significant differences between the mean electroactive surface area for different GO-concentrations within the same nanomaterial configuration. This indicates that the GO-concentration plays an important role on the electrochemical performance of the electrodes. For instance, the Pt/Ir–nPt–GO platform design with GO concentrations of 1 and 2 mg mL^{-1} produced cyclic voltammograms similar to those in Fig. 2A. However, the 3 mg mL^{-1} GO-concentration consistently produced sigmoidal voltammograms, which occur when the diffusion layer thickness is greater than the exposed surface area of the electrode. This indicates that the oxidative current reaches a steady state during the potential scan, impeding the formation of true redox peaks.[27]

The mean sensitivity towards H_2O_2 of all GO–Pt hybrids is presented in Fig. 5B. Similar to the trends from electroactive surface area, the Pt/Ir–GO platform configuration showed the lowest amperometric sensitivity (the average including all GO concentrations was 2.4 ± 1.2 μA Mm^{-1}), whereas the 2 mg mL^{-1}

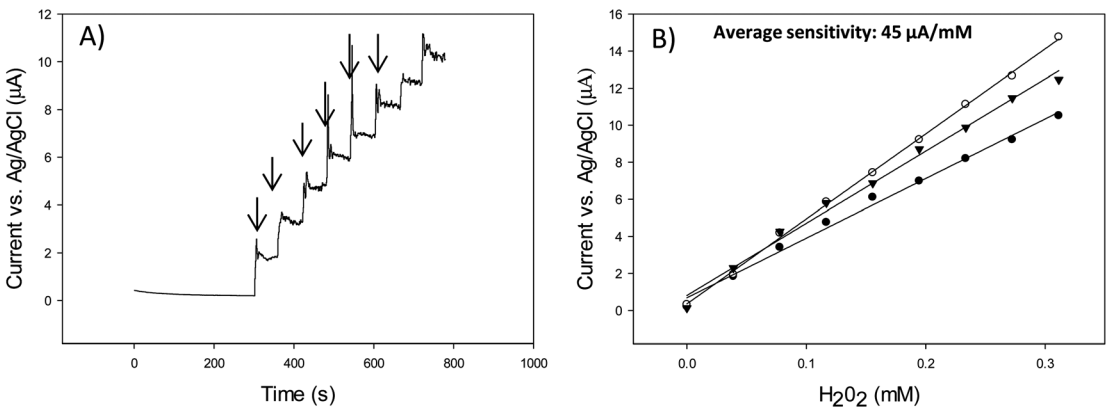

Fig. 3 (A) Representative DCPA curve showing the current response to successive injections of hydrogen peroxide (injection times are indicated by vertical arrows). (B) Characteristic calibration curves for the sensor. Each treatment was tested by triplicates.

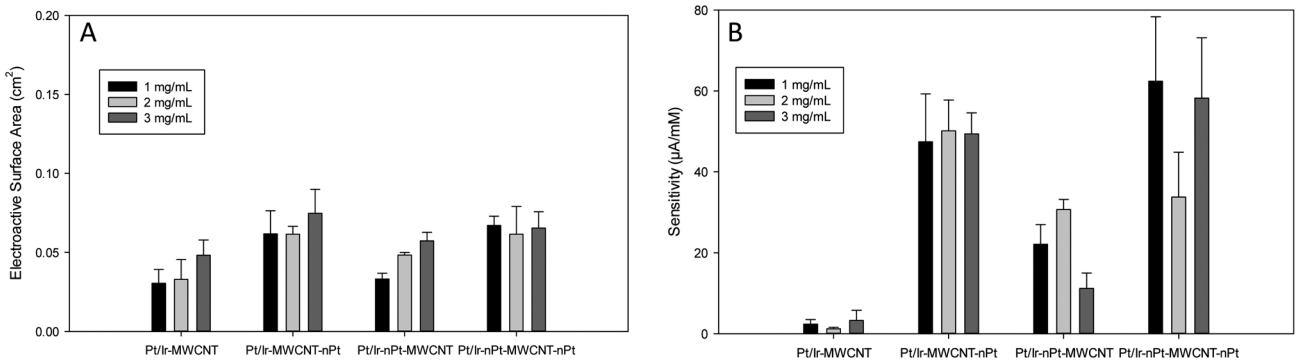

Fig. 4 Electrochemical performance of the MWCNT-based nanomaterial platforms. (A) Comparison between electroactive surface areas. (B) Comparison between sensitivities. Error bars denote the standard error of the arithmetic mean of the measurements ($n = 3$). Inset boxes indicate the concentration of MWCNT (panel A) or GO (panel B) used in combination with each nanomaterial configuration.

Pt/Ir–nPt–RGO–nPt modified electrode demonstrated the highest amperometric sensitivity of all the nanomaterial platforms tested (45 ± 3.2 μA mM^{-1}) being about 9 times better than a bare Pt/Ir electrode (4.9 ± 0.36 μA mM^{-1}).

Analysis of variance (ANOVA model I) was performed in order to determine whether or not any effects on the response variable (amperometric sensitivity) arising from the GO concentration or the platform configuration were statistically significant. A p-value smaller than the critical value ($p < 0.05$) was obtained for all factors including the interaction between GO concentration and platform configuration, indicating that there is a significant difference in amperometric sensitivity for at least one treatment of each factor (representative calibration curves of the GO-based nanomaterial platforms are available in ESI, Fig. 2†). A Tukey test was performed by simultaneously comparing the mean amperometric sensitivity of every factor level to the set of all pairwise comparisons. The four platform configurations were statistically different, and the mean sensitivity obtained using the 2 mg mL^{-1} GO concentration was significantly greater than the other concentrations tested. However, there was not a significant difference between the average sensitivities obtained with the 1 and 3 mg mL^{-1} GO concentrations (see ESI† data for interaction plots, Anova, and Tukey tables).

These results are consistent with other reports describing GO modified electrodes in the literature. Work by Kuila *et al.*[28] demonstrated how oxygen-containing functional groups on the basal planes and edges of GO sheets limit the electrocatalytic capabilities of this nanomaterial. Thus, GO must be reduced to enable the π–electronic conjugation. This explains the low electrocatalytic activity of the Pt/Ir–GO and Pt/Ir–nPt–GO platforms compared to the other two platform designs.

The Pt/Ir–RGO–nPt and Pt/Ir–nPt–RGO–nPt hybrid nanomaterials exhibited significantly improved electrochemical performance over all other carbon–metal nanohybrids in this study. Indeed, the electrodeposition of nPt onto GO must have two imperative effects on the electrocatalytic behavior of the platforms: (1) enhanced electronic π-conjugation due to GO reduction, and (2) integration of the nanomaterial platform by formation of metal junctions among GO sheets. These nanojunctions electrically connect the carbon–metal nanomaterial network, facilitating electron transport to the surface of the electrode. EDS analysis was used to confirm the partial removal of oxygen functionalities by electrodeposition of Pt

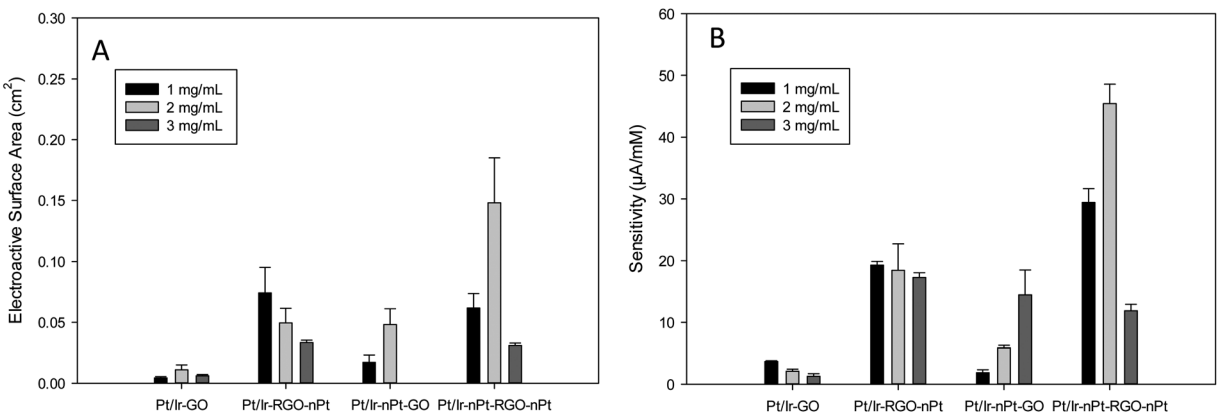

Fig. 5 Electrochemical performance of the GO-based nanomaterial platforms. (A) Comparison between electroactive surface areas. (B) Comparison between sensitivities. Error bars denote the standard error of the arithmetic mean of the measurements ($n = 3$). Inset boxes indicate the concentration of MWCNT (panel A) or GO (panel B) used in combination with each nanomaterial configuration.

nanoparticles on GO. As can be seen in Fig. 6, the atomic percent of oxygen in the Pt/Ir–nPt–RGO–nPt platform (21.4 at%) appears lower than the Pt/Ir–nPt–GO platform (43.2 at%).

This result is similar to the study by Wang *et al.*[29] Wang *et al.* demonstrated efficient reduction of GO during the synthesis of GO–nPt hybrids in chloroplatinic acid. Bonding of Pt nanoparticles onto reduced GO sheets prevents the aggregation of GO and maintains interplanar spacing. In another study, Guo *et al.*[30] reported the synthesis of high quality RGO nanosheets through electrochemical reduction of an exfoliated graphite oxide precursor material at cathodic potentials. Guo *et al.* concluded that the oxygen-containing functional groups were thoroughly removed from the graphite oxide plane *via* electrochemical reduction. Using a similar approach, An *et al.*[31] described an effective method for the simultaneous electrochemical reduction and electrophoretic deposition of reduced GO on various substrates including Cu, Ni, Al, stainless steel, and p-type Si. An *et al.* found that the electrophoretic deposition process successfully removed the oxygen functional groups in the GO film, improving its electrical conductivity.

Comparison of carbon–Pt hybrid nanocomposites

Fig. 7 shows the surface characteristics of the 2 mg mL^{-1} carbon–Pt nanocomposites "sandwich" designs using both SWLI and SEM. The morphology of the nPt–CNT hybrid structures are similar to those reported by McLamore *et al.*[11] and Shi *et al.*[12] (the structures in ref. 11 and 12 contained MWCNT directly cast onto electrodes). When compared to the graphene–Pt hybrids, the CNT–nPt nanostructures are heterogenous and have a relatively high degree of aggregation. The average surface roughness coefficient (rms) for the CNT–Pt

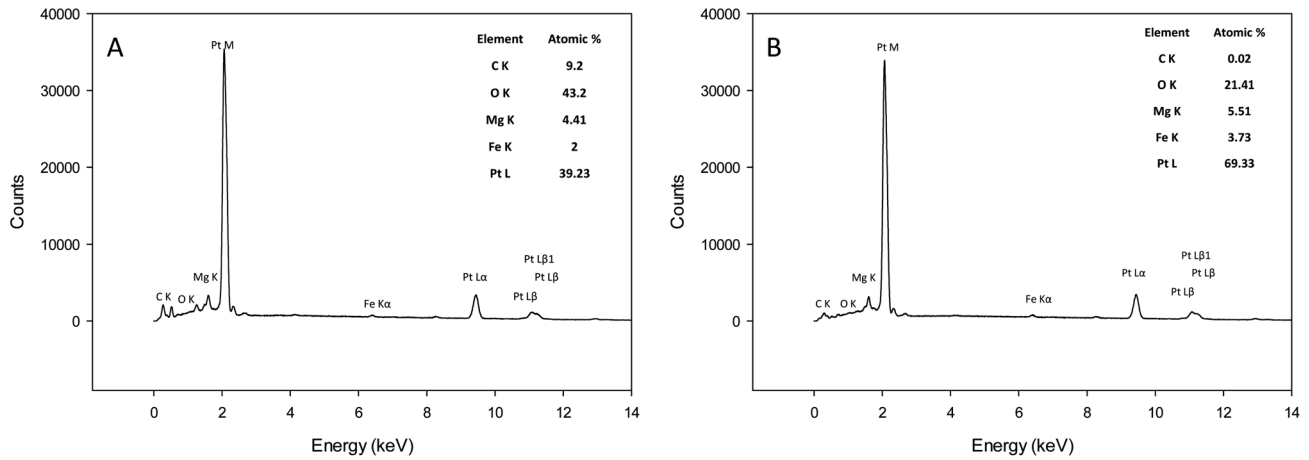

Fig. 6 (A) EDS spectrum of the 2 mg mL^{-1} Pt/Ir–nPt–GO nanomaterial platform. (B) EDS spectrum of the 2 mg mL^{-1} Pt/Ir–nPt–GO–nPt nanomaterial platform.

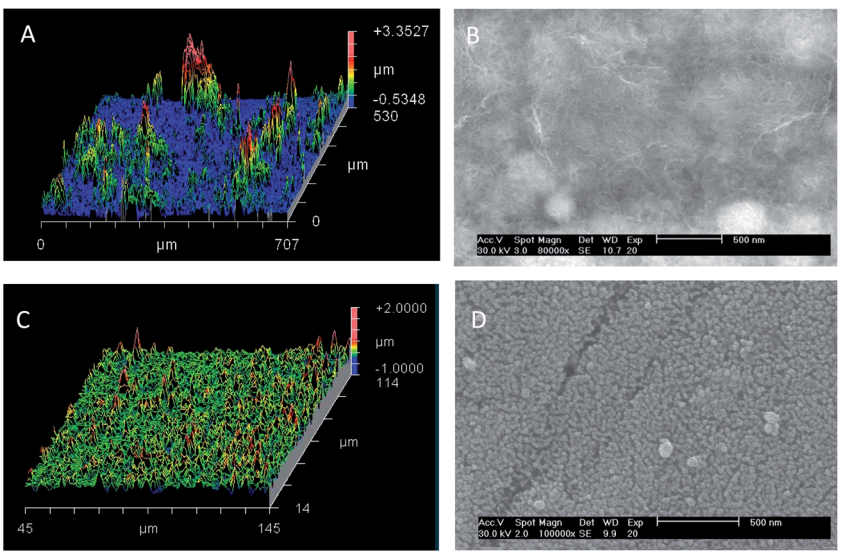

Fig. 7 Surface topography of 2 mg mL^{-1} CNT–Pt and graphene–Pt nanocomposites "sandwich" hybrids. (A) SWLI surface map of 707 × 530 µm area for MWCNT–Pt nanohybrid sandwich. (B) Representative SEM micrograph of MWCTN–Pt sandwich surface. (C) SWLI surface map of graphene–Pt hybrid for a 100 × 100 µm area. (D) Representative SEM micrograph of surface for RGO–Pt sandwich.

Table 1 Summary of some recent nanomaterial platform designs for amperometric sensors[a]

Platform	Sensitivity ($\mu A\ mM^{-1}$)	Response time (s)	LOD (μM)	Ref.
Pt/Ir–nPt–GO–nPt	45 ± 7	3 ± 22	0.14 ± 28	This work
Pt/Ir–MWCNT–nPt	49 ± 15	3 ± 14	0.43 ± 32	This work
Graphene–MWCNTs	$2.1 \pm$ NR	NR	9.4 ± 2.8	Woo *et al.*[32]
Graphene–CNT	$15 \pm$ NR	NR	$1 \pm$ NR	Dong *et al.*[33]
Graphene–AuNP	NR	$5 \pm$ NR	$0.22 \pm$ NR	Fang *et al.*[34]
GrOx–Pt black	4.8 ± 46	NR	NR	Shi *et al.*[11]
Nano-Pt	$9.15 \pm$ NR	NR	$5 \times 10^{-4} \pm$ NR	Chakraborty & Raj[35]

[a] NR = Not reported in manuscript.

nanocomposite "sandwich" was 303.3 nm. The surface map for the CNT–Pt nanohybrid shows a rough topography with peaks of irregular height distributed along the plotted area (Fig. 7A). Mono-dispersed deposits of amorphous platinum-black can be seen in the SEM micrograph shown in Fig. 7B. The irregular structure is likely due to poor stacking of MWCNT within the nanohybrid when compared to graphene stacking. The root mean square surface roughness coefficient for reduced graphene–Pt nanohybrids (166.5 nm) was significantly lower than the MWCNT–Pt hybrid sandwich design (Fig. 7C). Together with the enhanced electrocatalytic behavior of RGO relative to MWCNT (Fig. 4 and 5), this indicates that RGO sheets were stacked in a semi-ordered manner between the nPt clusters. SEM images of the RGO–Pt nanohybrid show this smooth stacking and homogenous distribution of nPt along the RGO sheets (Fig. 7D and also EDS data in Fig. 6). The morphology of CNT and graphene structures formed through chemical vapor deposition (CVD) of plasma vapor deposition (PVD) is much more homogenous than the structures formed in these studies.[9,11,16] Thus, one would expect the performance of CVD or PVD-derived nanocomposites to be far superior to the nanocomposites developed in this study using facile methods. However, when a "sandwich" hybrid nanostructure is created the electron transport is competitive with CVD and PVD formed nanocomposites.

Table 1 summarizes the performance characteristics of GO and MWCNT hybrid nanocomposites from this study and similar platforms for amperometric sensors in the literature.[11,32–35] As listed in this table, the amperometric sensitivity towards hydrogen peroxide has been greatly improved by the Pt/Ir–MWCNT–nPt and Pt/Ir–nPt–RGO–nPt nanohybrids compared to previous reports. Other performance characteristics (response time, selectivity, limit of detection) for the recipes here are within the range found in the literature. The nanomaterial deposition methodology described in this paper is a simple, fast, and efficient approach for the fabrication of electrocatalytic platforms for amperometric sensors and biosensors. Importantly, the recipe uses commonly available equipment and chemicals, ensuring the methods can be reproduced in any sensor lab. This facile graph-onto methodology is highly efficient and competes with relatively complex graph-from synthesis of carbon–metal hybrid nanocomposites.

Conclusions

A facile approach for the fabrication of hybrid nanocomposites based on mutiwalled carbon nanotubes, graphene oxide, and nanoplatinum was demonstrated. The effect of carbon concentration and network configuration on electrochemical performance was studied in detail. For the GO–Pt nanohybrids, both design factors played a major role on electrocatalytic response. On the other hand, performance characteristics of the MWCNT nanohybrids were only affected by the configuration factor, and MWCNT concentration in the range of 1 to 3 mg mL^{-1} did not have an effect on performance. The network configuration factor affected the electrochemical performance of both GO-based and CNT-based electrodes in a similar manner since in both cases the nanomaterial platforms with nPt on the top layer showed a significantly enhanced amperometric sensitivity compared to the platform configurations with either GO or CNTs on top. This effect was namely attributed to the electrical integration by formation of metal junctions among GO sheets or CNTs. Conversely, the carbon concentration variable in the tested range affected the GO-based and CNT-based electrodes differently. We assume this occurs because the critical concentration of these two materials is inherently different. In the GO case, a low carbon concentration (*e.g.* 1 mg mL^{-1}) resulted in isolated sheets deposited in random orientations leading to a poor electronic conjugation to the electrode's surface; in the other hand, a large concentration (*e.g.* 3 mg mL^{-1}) resulted in stacking of GO sheets turning them into graphitic structures with lower electrical conductivity. Thus, there was a middle point where enhanced electrochemical performance was achieved (*e.g.* 2 mg mL^{-1}). We believe that a similar effect (with an optimal carbon concentration) could be observed with CNTs, but perhaps in a wider concentration range.

Some of the reduced GO and MWCNT-nanocomposite platforms show promising potential for the development of highly sensitive amperometric biosensors. Future enhancements to the GO-based platforms may include further removal of oxygen functional groups by a low-cost/environmentally-friendly reducing agent such as magnesium chloride or ascorbic acid.

Acknowledgements

The authors would like to thank the Colombian funding agencies Colfuturo and Colciencias, the Agricultural and Biological Engineering Department of the University of Florida, the FAMU Feeder Program, and the UF Early Career Award for the financial support.

References

1 A. Chen and S. Chatterjee, *Chem. Soc. Rev.*, 2013, **42**(12), 5425–5438.
2 J. J. Gooding, *Electrochim. Acta*, 2005, **50**(15), 3049–3060.
3 D. Hernandez-Santos, M. B. Gonzalez-Garcia and A. Costa-Garcia, *Electroanalysis*, 2002, **14**(18), 1225–1235.
4 Y. Shao, J. Wang, H. Wu, J. Liu, I. A. Aksay and Y. Lin, *Electroanalysis*, 2010, **22**(10), 1027–1036.
5 A. K. Geim and K. S. Novoselov, *Nat. Mater.*, 2007, **6**, 183–191.
6 Z. J. Fan, J. Yan, T. Wei, G. Q. Ning, L. J. Zhi, J. C. Liu, D. X. Cao, G. L. Wang and F. Wei, *ACS Nano*, 2011, **5**, 2787–2794.
7 S. Stankovich, D. a. Dikin, G. H. B. Dommett, K. M. Kohlhaas, E. J. Zimney, E. a. Stach, R. D. Piner, S. T. Nguyen and R. S. Ruoff, *Nature*, 2006, **442**, 282–286.
8 R. Muszynski, B. Seger and P. V. Kamat, *J. Phys. Chem. C*, 2008, **112**, 5263–5266.
9 J. C. Claussen, S. S. Kim, A. U. Haque, M. S. Artiles, D. M. Porterfield and T. S. Fisher, *J. Diabetes Sci. Technol.*, 2010, **4**(2), 312–319.
10 L. Han, Q. Wang, S. Tricard, J. Liu, J. Fang, J. Zhao and W. Shen, *RSC Adv.*, 2013, **3**(1), 281.
11 E. S. McLamore, J. Shi, D. Jaroch, J. C. Claussen, A. Uchida, Y. Jiang, W. Zhang, S. S. Donkin, M. K. Banks, K. K. Buhman, D. Teegarden, J. L. Rickus and D. M. Porterfield, *Biosens. Bioelectron.*, 2011, **26**(5), 2237–2245.
12 J. Shi, E. S. McLamore and D. M. Porterfield, *Biosens. Bioelectron.*, 2013, **40**(1), 127–134.
13 Y. C. Tsai and Y. H. Hong, *J. Solid State Electrochem.*, 2008, **12**(10), 1293–1299.
14 B. L. Huang and C. Y. Mou, *Europhys. Lett.*, 2009, **88**(6), 68005.
15 J. Shi, H. Zhang, A. Snyder, M. Wang, J. Xie, D. M. Porterfield and L. A. Stanciu, *Biosens. Bioelectron.*, 2012, **38**(1), 314–320.
16 J. C. Claussen, M. S. Artiles, E. S. McLamore, S. Mohanty, J. Shi, J. L. Rickus, T. S. Fisher and D. M. Porterfield, *J. Mater. Chem.*, 2011, **21**(30), 11224.
17 J. Shi, J. C. Claussen, E. S. McLamore, A. ul Haque, D. Jaroch, A. R. Diggs, P. Calvo-Marzal, J. L. Rickus and D. M. Porterfield, *Nanotechnology*, 2011, **22**(35), 355502.
18 J. Wang, *Analytical electrochemistry*, John Wiley & Sons, Inc., New York, 3rd edn, 2006.
19 IUPAC Compendium of Chemical Terminology, in *IUPAC Gold Book*, 2012, p. 3540, DOI: 10.1351/goldbook.L03540.
20 D. Diamond, *Principles of Chemical and Biological Sensors*, ed. J. D. Winefordner, John Wiley & Sons, Inc., New York, 1st edn, 1998, vol. 150.
21 L. Ott, *An introduction to statistical methods and data analysis*, Wadsworth, Inc., Belmont, Ca, 4th edn, 1993.
22 X. Chu, D. Duan, G. Shen and R. Yu, *Talanta*, 2007, **71**(5), 2040–2047.
23 J. Wang, S. Yang, D. Guo, P. Yu, D. Li, J. Ye and L. Mao, *Electrochem. Commun.*, 2009, **11**(10), 1892–1895.
24 S. Ilani and P. L. McEuen, *Annu. Rev. Condens. Matter Phys.*, 2010, **1**(1), 1–25.
25 A. B. Kaiser and V. Skákalová, *Chem. Soc. Rev.*, 2011, **40**(7), 3786–3801.
26 J. Svensson and E. E. B. Campbell, *J. Appl. Phys.*, 2011, **110**(111101), 1–16.
27 A. J. Bard and L. R. Faulkner, *Electrochemical methods: fundamentals and applications*, John Wiley & Sons, Inc., New York, 2nd edn, 2001.
28 T. Kuila, A. K. Mishra, P. Khanra, N. H. Kim and J. H. Lee, *Nanoscale*, 2013, **5**(1), 52–71.
29 Y. Wang, J. Liu, L. Liu and D. D. Sun, *Nanoscale Res. Lett.*, 2011, **6**(1), 241.
30 H. L. Guo, X. F. Wang, Q. Y. Qian, F. B. Wang and X. H. Xia, *ACS Nano*, 2009, **3**(9), 2653–2659.
31 S. J. An, Y. Zhu, S. H. Lee, M. D. Stoller, T. Emilsson, S. Park, A. Velamakanni, J. An and R. S. Ruoff, *J. Phys. Chem. Lett.*, 2010, **1**(8), 1259–1263.
32 S. Woo, Y. R. Kim, T. D. Chung, Y. Piao and H. Kim, *Electrochim. Acta*, 2012, **59**, 509–514.
33 X. Dong, Y. Ma, G. Zhu, Y. Huang, J. Wang, M. B. Chan-Park, L. Wang, W. Huang and P. Chen, *J. Mater. Chem.*, 2012, **22**(33), 17044.
34 Y. Fang, S. Guo, C. Zhu, Y. Zhai and E. Wang, *Langmuir*, 2010, **26**(13), 11277–11282.
35 S. Chakraborty and C. R. Raj, *Biosens. Bioelectron.*, 2009, **24**(11), 3264–3268.